

Topologically protected quantum bits from Josephson junction arrays

L.B. Ioffe^{*,‡}, M.V. Feigel'man[‡], A. Iosevich[‡], D. Ivanov[†], M. Troyer[†], and G. Blatter[†]

^{*}*Department of Physics and Astronomy, Rutgers University, Piscataway, NJ 08854, USA*

[‡]*Landau Institute for Theoretical Physics, 117940 Moscow, Russia*

[†]*Theoretische Physik, ETH-Hönggerberg, CH-8093 Zürich, Switzerland*

(November 9, 2001)

All physical implementations of quantum bits (qubits), carrying the information and computation in a putative quantum computer, have to meet the conflicting requirements of environmental decoupling while remaining manipulable through designed external signals. Proposals based on quantum optics naturally emphasize the aspect of optimal isolation [1–3], while those following the solid state route exploit the variability and scalability of modern nanoscale fabrication techniques [4–8]. Recently, various designs using superconducting structures have been successfully tested for quantum coherent operation [9–11], however, the ultimate goal of reaching coherent evolution over thousands of elementary operations remains a formidable task. Protecting qubits from decoherence by exploiting topological stability, a qualitatively new proposal due to Kitaev [12], holds the promise for long decoherence times, but its practical physical implementation has remained unclear so far. Here, we show how strongly correlated systems developing an isolated two-fold degenerate quantum dimer liquid groundstate can be used in the construction of topologically stable qubits and discuss their implementation using Josephson junction arrays.

Any quantum computer has to incorporate some fault tolerance as we cannot hope to eliminate all the various sources of decoherence. Amazing progress has been made in the development of quantum error correction schemes [13] which are based on redundant multi-qubit encoding of the quantum data combined with error detection- and recovery steps through appropriate manipulation of the data. Error correction schemes are generic (and hence are applicable to any hardware implementation), but require repeated active interference with the computer during run-time; the delocalization of the data, often in a hierarchical structure, boosts the system size by a factor 10^2 to 10^3 . Delocalization of the quantum information is also at the heart of topological quantum computing [12], however, the stabilization against decoherence is entirely deferred to the hardware level (hence it is tied to the specific implementation) and is achieved passively. In searching for a physical implementation of topological qubits one strives for an extended (many body) quantum system where the Hilbert space of quantum states decomposes into mutually orthogonal sectors, each sector remaining isolated under the action of local pertur-

bations. Choosing the two qubit states from groundstates in different sectors protects these states from unwanted mixing through noise; protection from leakage within the sector has to be secured through a gapped excitation spectrum. As no local operator can interfere with these states, global operators must be found (and implemented) allowing for the manipulation of the qubit state.

A promising candidate fulfilling the above requirements is the quantum dimer system [14–16]: recent quantum Monte Carlo simulations of the dimer model on a triangular lattice provide evidence for a gapped liquid groundstate [17] (see [18,19] for a discussion of similar exotic groundstates in spin models) and we will discuss its topological robustness below. The physical implementation of such a dimer system can be realized with the help of quantum Josephson junction arrays. Such arrays allow for a proper ‘material design’ as the energy scales governing the charge and phase degrees of freedom can be tuned through junctions with appropriate tunnel barriers and capacitances. Shaped into the form of a ring, the Josephson junction array emulating a dimer system allows for the construction of topologically protected qubits.

The simplest dimer model is defined on a square lattice; allowed configurations are coverings with dimers connecting neighboring vertices satisfying the constraint that every vertex belongs to only one dimer, see Fig. 1. Attributing equal energies to these states, the classical model is characterized by an extensive entropy. The quantum dynamics is introduced by the hopping Hamiltonian

$$H_t = -t \sum_{\square} (| \uparrow \rangle \langle \downarrow | + | \downarrow \rangle \langle \uparrow |) \quad (1)$$

rotating parallel dimers on appropriate plaquettes \square . As a result, the degeneracy of the classical model is lifted, with ‘columnar’ and ‘staggered’ (e.g., brickwall) phases (see Fig. 1) assuming minimal and maximal energies, respectively. In order to avoid such crystalline ordering we frustrate parallel dimers with the interaction term

$$H_v = v \sum_{\square} (| \uparrow \rangle \langle \uparrow | + | \downarrow \rangle \langle \downarrow |). \quad (2)$$

At $t = v$ (the Rokhsar-Kivelson point) a zero energy dimer liquid groundstate is formed involving all allowed configurations with equal amplitudes [15]. For the square lattice this liquid phase is restricted to the point $t = v$ and tuning v away from t the liquid loses the competition with various crystalline phases [20]. Here, we are

interested in systems developing a stable liquid over an extended parameter range. Such a stabilization may be achieved by the term

$$H_d = \sum_{\square} [-t(|-\rangle\langle\prime\prime| + |'\rangle\langle\prime| + h.c.) + \mu|\prime\rangle\langle\prime|] \quad (3)$$

transforming horizontally ($|-\rangle$) and vertically ($|'\rangle$) shifted dimers into diagonal ones $|\prime\rangle$ at the energy cost 2μ (only one family of diagonals is chosen). Tuning the chemical potential μ from ∞ to 0, diagonal dimer flips proliferate and we can study the evolution of the dimer model as we go from a square to a triangular lattice [21].

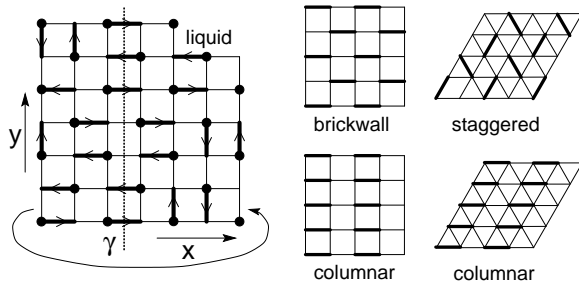


FIG. 1. Dimers on a square lattice forming liquid (main panel), brickwall, and columnar configurations. Periodic boundary conditions are applied along the x -direction. The sublattice A is marked by solid bullets; dimers are attributed a direction pointing away from bullets. The topological invariant ϕ counts the number of dimers crossing the reference line γ , with dimers pointing to the right (left) counting with positive (negative) signs (here, $\phi = 1$). Right: staggered and columnar configurations in the triangular lattice.

The above type of quantum dimer models has been actively discussed in the context of short-range resonating-valence-bond (RVB) models [22] for high temperature superconductivity [14]. In order to gain more insight into its physical properties we exploit a mapping to an ‘electrodynamic’ analogue [20,21,23]: We decorate the bipartite square lattice (sublattices A and B) with static charges $\rho_{\square} = \pm 1$, placing all positive charges on the sublattice A , see Fig. 1. A dimer covering $\{\mathbf{d}_{\langle i,j \rangle}\}$ of bonds $\langle i,j \rangle$ of this ‘ionic crystal’ is mapped to a distribution of electric dipoles $\{-\mathbf{p}_{\langle i,j \rangle}\}$; the electric field $\mathbf{e} = -\langle \mathbf{p}_{\langle i,j \rangle} \rangle_{\delta A}$ resulting from averaging over small areas δA then satisfies Gauss’ law $\nabla \cdot \mathbf{e} = \langle \rho \rangle_{\delta A} = 0$. The simplest dynamics preserving this constraint is given by Faradays law or, more precisely, (compact) quantum electrodynamics. Here, we are interested in the large-scale (global) aspects of the model and hence we will keep the discussion on a phenomenological level; the physical properties of the dimer liquid phase will be described in terms of the electric field \mathbf{e} and the dielectric constant ε .

While the order characterizing the crystal phases is obvious, the topological order present in the dimer liquid phase is more subtle [14–16]: we consider a cylindrical geometry with periodic boundary conditions along the

x -axis, leaving the boundaries along the y -direction free (an additional periodic boundary condition along the y -direction defines a torus, see later). In the absence of diagonal dimers (the limit $\mu \rightarrow \infty$ in (3)) the sum ϕ counting directed dimers cut by the reference line γ parallel to the y -axis defines a topological order parameter (dimers pointing into opposite directions are counted with opposite sign): the action of the Hamiltonian $H = H_t + H_v$ leaves ϕ invariant and the Hilbert space splits into topological sectors \mathcal{H}_{ϕ} characterized by the integers ϕ . Within our electrodynamic analogue this topological invariant is given by the flux $\phi = \int dy \varepsilon e_x$ of the electric induction across γ and each sector \mathcal{H}_{ϕ} is characterized by an average polarization $e_x = \phi / \varepsilon L_y$ producing a groundstate energy $E = \varepsilon e^2 L_x L_y / 2 = \phi^2 L_x / 2 \varepsilon L_y \equiv E_{\phi}$. At finite values of the chemical potential μ the Hamiltonian (3) introduces mobile defects with charge ± 2 [21,24]. These charges mix states with electric flux $\phi \pm 2$: creating two defects of charge ± 2 , carrying one defect around the cylinder, and subsequent annihilation with its partner changes the flux ϕ by 2; as a result, the infinite set of sectors \mathcal{H}_{ϕ} collapses to the even and odd sectors $\mathcal{H}_{e,o}$.

The Hamiltonian projected onto the space of ground states within topological sectors \mathcal{H}_{ϕ} takes the form $H_{\text{sec}} = \sum_{\phi} (E_{\phi} |\phi\rangle\langle\phi| + J(|\phi\rangle\langle\phi+2| + h.c.))$. For large values of the chemical potential $\mu \gg t$ the defect pairs are only virtual and the amplitude J mixing states with different ϕ is exponentially small in the circumference L_x , $J \propto (t/\mu)^{L_x}$.

As μ drops below an energy of order t , defects proliferate and undergo Bose condensation; the concomitant long range order in the condensate phase φ implies large charge fluctuations and thus the electric field flux across γ fluctuates strongly. In this phase the mixing between sectors is large with $\langle \phi^2 \rangle \propto L_y$: assuming a superfluid density ρ_s , the hydrodynamic description of the charged superfluid [23] is given by the Euclidean action (in Fourier space; ρ denotes the conjugate to φ) $S_E = \sum_{\omega, \mathbf{k}} [\omega \rho_{-\omega, -\mathbf{k}} \varphi_{\omega, \mathbf{k}} + \rho_s K^2 |\varphi_{\omega, \mathbf{k}}|^2 / 2 + |\rho_{\omega, \mathbf{k}}|^2 / 2 \varepsilon K^2]$, from which we derive a density correlator $\langle \rho \rho \rangle = \rho_s K^2 / (\rho_s / \varepsilon + \omega^2)$. The relation $\varepsilon \nabla \cdot \mathbf{e} = \rho$ allows us to find the equal time correlator of the electric induction $\langle \varepsilon e_{\mu}(\mathbf{R}, t) \varepsilon e_{\nu}(\mathbf{R}', t) \rangle = \delta_{\mu\nu} \delta^2(\mathbf{R} - \mathbf{R}') \sqrt{\rho_s \varepsilon} / 2$, resulting in the mean electric flux $\langle \phi^2 \rangle = \sqrt{\rho_s \varepsilon} L_y / 2$ crossing the line γ ; the local correlations in the electric field are a consequence of the dispersion-free plasmon spectrum.

The new groundstates $|e, o\rangle \propto \sum_{\phi_{e,o}} a_{\phi_{e,o}} |\phi_{e,o}\rangle$ involve contributions from all sectors $\mathcal{H}_{e,o}$, with $\phi_e = 2k$ and $\phi_o = 2k + 1$ running over even and odd integers; their physical properties are conveniently characterized by the distribution function $P(\phi) = |a_{\phi}|^2 \propto \exp(-\phi^2 / 2\sigma)$, with the Gaussian form appropriate for a process involving a sum of statistically independent elements. The width σ is obtained through a comparison with the second moment $\langle \phi^2 \rangle$, $\sigma = \sqrt{\rho_s \varepsilon} L_y / 2$. Expectation values in even

and odd sectors $\mathcal{H}_{e,o}$ are given by the sums over even and odd ϕ with weight $P(\phi)$. As a result, differences between expectation values in $\mathcal{H}_{e,o}$ are exponentially small in L_y , e.g., the average squares of electric fluxes differ by

$$\langle \phi^2 \rangle_e - \langle \phi^2 \rangle_o \sim \exp(-\pi^2 \sqrt{\rho_s \varepsilon} L_y / 4). \quad (4)$$

Hence, the presence of diagonal dimers provides us with only two topological sectors for a system defined on a cylinder (and 4 sectors on a torus). The corresponding groundstates are degenerate in the limit $L_{x,y} \rightarrow \infty$. Finite-size effects as well as local disorder lead to an exponentially weak energy splitting (cf. (4)). Furthermore, the topological property of the system inhibits any mixing of the two groundstates. In the thermodynamic limit the collapse of infinitely many to two topological sectors involves a quantum phase transition in the parameter μ . For $\mu = 0$ the above model corresponds to a symmetric triangular lattice (upon including the v -term) and we expect favorable conditions for the construction of protected qubits.

Indeed, this expectation is supported by results obtained from numerical studies: recent Monte Carlo simulations by Moessner and Sondhi [17] on large systems with $L_{x,y} = 36$ exhibit short-range dimer-dimer correlations within a parameter region $2/3 < v/t < 1$, indicative of a liquid state. Furthermore, the weak temperature dependence of this data within the temperature interval $0.25t > T > 0.03t$ provides evidence for a gapped spectrum (increasing v beyond t , a first-order transition takes the liquid into the staggered phase, while decreasing v below $2t/3$ establishes some crystalline order).

We have numerically diagonalized the t - v dimer Hamiltonian $H = H_t + H_v$ on a triangular lattice in order to estimate the gap protecting the liquid and verify the absence of low lying edge states; in addition we have investigated the robustness of the degenerate groundstates under local perturbations (requiring exact diagonalization limited to smaller systems). We have chosen both cylindrical and toroidal geometries, with system sizes going up to $L_{x,y} = 6$; although subject to finite size effects we expect that our approach describes well the liquid phase where the short-ranged dimer correlations (of order of one lattice constant [17]) reduce the influence of the boundaries. Our exact diagonalization study confirms the presence of a gap of order $\Delta \approx 0.1t$, taking up large values on approaching the Rokhsar-Kivelson point $t = v$. Comparing the spectra for tori (no open boundaries) with those of cylinders (where the two open boundaries could accommodate edge states, would they exist) we note that the gap persists, from which we infer the absence of low lying edge-states in the dimer liquid (this should be contrasted with the situation in the quantum Hall system).

In order to test the susceptibility of the degenerate groundstates to local perturbations we assign all

links random chemical potentials μ_d homogeneously distributed over the interval $[-d/2, d/2]$, $d < t$. In finite cylinders and tori, particular symmetries specific to some geometries $L_{x,y}$ produce an exact degeneracy of eigenstates from different topological classes; for the 6×5 cylinder and torus used in our study the symmetry analysis predicts double-degeneracy. As shown in Fig. 2 the disorder induced groundstate splitting Δ_d collapses dramatically as we go from the crystal ($v > t$) to the liquid phase ($v < t$) and slowly recovers as v is decreased further. We attribute the sharp drop at $v \approx t$ to the first-order solid-liquid transition; the small disorder splitting at $v < t$ testifies for the efficient protection of the dimer liquid groundstates from local perturbations. Decreasing v further below t we observe level crossings which we attribute to the appearance of intermediate crystalline phases [17] before reaching the fluctuating columnar phase at large negative values of v .

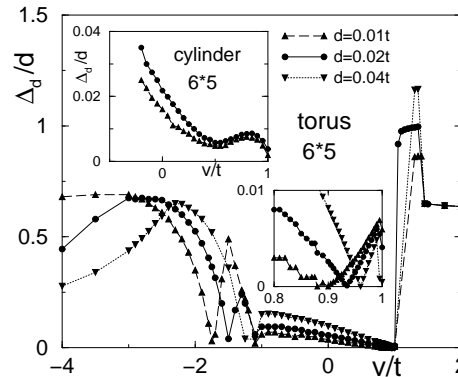


FIG. 2. Splitting Δ_d of the groundstate energies under the action of a disorder potential of strength d for a 6×5 torus and a 6×5 cylinder (inset; periodicity is along x with $L_x = 6$). The disorder only weakly perturbs the dimer liquid groundstates at $v < t$ (note the expanded view near $v \sim t$ for the 6×5 torus). The crossovers between various phases become clearly visible in the susceptibility to a disorder potential.

Summarizing, the combination of Monte Carlo simulations [17] and diagonalization indicate that on approaching the point $v = t$ from below, the triangular dimer model develops an isolated degenerate dimer liquid groundstate free of edge states. Within the parameter region $\sim 0.8 < v/t < 1$ we find a gap of order $0.1t$ and groundstates which are robust under disorder to within 1% of the disorder potential; we expect a further increase of this robustness with system size, cf. (4). Translating these findings to potential implementations of this two-state system, we find the latter to be quite tolerant with respect to (static) local variations in parameters appearing in the fabrication process. Regarding decoherence, the amplitude mixing of the two groundstates is strongly suppressed, since it involves creation of topological defects (real or virtual) violating the dimer constraint. The decoherence in the relative phase of the two groundstates originates either from their adiabatic

splitting by an external low-frequency noise, or the creation of non-topological excitations within each sector. The former is suppressed for the same reason that leads to the robustness with respect to local disorder, while the latter is inhibited by the gap Δ , which sets the requirement $T \ll \Delta$ on the operation temperature.

In the following we propose two types of Josephson junction arrays for the implementation of the above topologically protected quantum dimer liquid groundstates and their use for quantum computing. In the first array (JJT), the vertices of the triangular lattice are structured into six Y-shaped superconducting islands with two ends joining into the hexagonal vertex and the third end linking to the neighboring hexagon, see Fig. 3. The 5 parameters, the capacitance C_Y of the island to the groundplate, the capacitance C_h and Josephson current I_h of the hexagonal vertex junction, and the capacitance C_l and Josephson current I_l of the link junction, are chosen to emulate the triangular quantum dimer model. All capacitances and currents define corresponding energies $E^C = e^2/2C$ and $E^J = \Phi_0 I/2\pi c$, where $\Phi_0 = hc/2e$ denotes the flux quantum (e.g., $E_h^C = (2e)^2/2C_h$, $E_h^J = \Phi_0 I_h/2\pi c$). We first find C_Y , C_h , and I_l defining the classical dimer states: We choose a large capacitance C_h in order to join the islands electrically into one hexagonal vertex. A small capacitance C_Y defines the large charging energy $E_{\text{hex}} \approx E_Y^C/6$ of the hexagonal vertex, the basic energy scale of the array. We introduce ‘charge frustration’ of the vertices by biasing the array with a global electric gate such as to equalize the energies (to an accuracy better than E_l^J) of two states differing by one Cooper pair (this defines a ‘half-filled’ array); the large charging energy E_{hex} lifts other charge states to high energies. The Cooper pairs lower their energy via tunneling (involving the coupling I_l) through the link junction joining two vertices — the ‘bonding’ state of such a Cooper pair defines the dimer state. With only half a Cooper-pair available per hexagonal vertex, each vertex is involved in the formation of one and only one of these ‘valence bonds’. This defines the ‘classical’ configurations of the dimer model; the corresponding Hilbert space of dimer states is protected by the energy scale E_l^J .

The dimer dynamics involves the vertex junction and proceeds via localization of one dimer to the vertex (with an energy cost E_l^J) and subsequent hops (of two parallel dimers/Cooper pairs over junctions with energy E_h^J , see Fig. 3) to the new vertex islands. The hopping amplitude is of order $t \sim E_h^{J2}/E_l^J$; explicit calculation gives the result $t = (9/16)E_h^{J2}/E_l^J$. The electrostatic interaction between dimers depends on the choice of the capacitance matrix and its dependence on the dimer configuration is non-trivial. First, we compare the energies of the staggered and columnar configurations and find the interaction energy v between parallel dimers; in the limit $C_l \ll C_Y, C_h$, $v = E_h^C(C_l/C_h)[(1 + C_Y/C_h)(1 + 3C_Y/C_h)]^{-2}$. Second, we have checked that the electrostatic energies

of the liquid phase dimer configurations indeed scale (to within $\sim 5\%$ accuracy) with the number of parallel dimer pairs. The condition $C_l \ll C_Y$ guarantees a short range interaction between dimers.

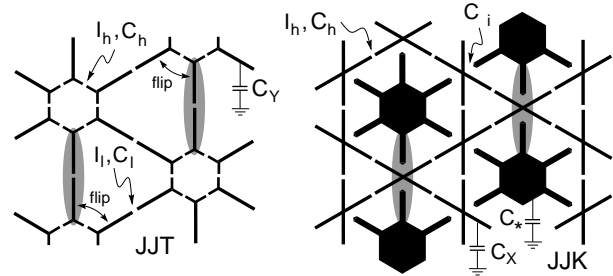


FIG. 3. Josephson junctions arrays forming triangular (JJT) and Kagome (JJK) lattices and emulating dimer systems. JJT: The large capacitance C_h joins hexagonal islands into electric units which are frustrated by a global gate to accept $1/2$ Cooper pair. Cooper pairs resonating between hexagonal islands form dimers (shaded ellipses); dimer flips due to H_t are indicated by arrows. JJK: Cooper pairs on X-shaped islands are capacitively coupled through star-shaped islands. The gate is tuned to allow for $1/2$ Cooper pair per hexagon. Dimers are pairs residing on X-shaped islands and polarizing adjacent star-shaped islands.

The backbone of the second array (JJK) is made from X-shaped islands arranged into a Kagome lattice with capacitive and Josephson couplings E_h^C and E_h^J , see Fig. 3. A second triangular lattice of star-shaped islands introduced into the hexagons of the Kagome lattice is only capacitively coupled (with energy E_i^C) to the islands of the Kagome lattice; C_X and C_* denote the capacitances of the islands to the ground. The Kagome sites are biased with a global external gate to accept one additional Cooper pair per hexagon at equal energy, resulting in a filling with $1/2$ Cooper pair per hexagon. The similarity between the Kagome lattice and the triangular array becomes obvious when joining pairs of Y-shaped islands (corresponding to the limit $C_l \rightarrow \infty$ and $I_l \rightarrow \infty$) and contracting the link to obtain the X-shaped island — the previous vertex junctions now play the role of the junctions on the Kagome lattice, hence the same index ‘ h ’ has been chosen for the junctions on the hexagons; note that the present array involves only one type of Josephson junctions. By analogy, dimers now correspond to Cooper pairs localized onto the X-islands of the Kagome lattice. As dimers should not touch one another, no two bosons are allowed on the same hexagon: We choose small capacitances C_h in order to isolate hexagons from one another (note the difference to the JJT array) and large capacitances C_i to join the six X-shaped islands forming the hexagon into one electrostatic unit via their strong coupling to the central star-shaped island. The capacitances C_X , C_* , and C_i then define the charging energy required to put two Cooper pairs on the same hexagon, $E_{\text{hex}} \approx (C_i/C_X)^2 E_*^C$, which is our basic energy scale (we

assume $C_i < C_*$, C_x in order to guarantee good screening on large distances).

The motion of the Cooper pairs (the dimer dynamics) involves the hopping amplitude E_h^J and the charging energy E_{hex} of the virtual state with two Cooper pairs on the same hexagon, $t \sim E_h^J/E_{\text{hex}}$; note that we require $E_h^J \ll E_{\text{hex}}$ not to perturb the proper frustration of the array. The interaction energy v again derives from a comparison between the staggered and columnar states and has to meet the conflicting requirements of increasing the energy of parallel dimers (next-nearest neighbor interaction) while leaving non-parallel dimer pairs (next-next-nearest neighbor interaction) approximately unperturbed. In order to produce a positive v we need a finite coupling C_h , which in turn reduces the basic energy E_{hex} . We find that the set $5C_i = C_* = C_x = 20C_h$ produces a (renormalized) protective energy $E_{\text{hex}}^r \approx 0.008E_*^c \approx 0.2E_{\text{hex}}$ and a repulsive energy $v \approx 0.1E_{\text{hex}}^r$. Choosing $E_h^J \approx 0.3E_{\text{hex}}^r$ we can properly satisfy the condition $t \approx v$.

We construct a topologically protected qubit from the two-level system defined by the two ground states of a quantum dimer system with cylindrical boundary conditions. We make use of the above Josephson junction arrays and a ring geometry; the two qubit states $|e\rangle$ and $|o\rangle$ then are distinct through the parity of the dimer count along the line γ joining the inner and outer boundaries of the array, see Fig. 4. In order to manipulate the qubit we have to implement the qubit Hamiltonian

$$H_{\text{qubit}} = h_x \sigma_x + h_z \sigma_z, \quad (5)$$

where σ_x and σ_z are Pauli matrices and h_x , h_z are the (manipulable) parameters producing the amplitude (α) and phase (χ) mixing in the qubit state $|\alpha, \chi\rangle = [|e\rangle + \alpha \exp(i\chi)|o\rangle] / \sqrt{1 + \alpha^2}$. The implementation of h_x requires a controlled mixing of the protected dimer states, implying a reduction of the ground state's topological protection. In the JJT array this is achieved by breaking one dimer bond and creation of a virtual particle-hole excitation where one Cooper pair retreats to one hexagon (particle), leaving the partner hexagon empty (hole). This virtual excitation costs the energy \tilde{E}_l^J of that particular bond and takes the system (virtually) out of the protected dimer space. While the particle remains pinned to the weak junction, the hole is taken around the inner boundary through appropriate dimer flips and is subsequently recombined with the particle. This process results in a mixing amplitude $h_x \sim E_h^J (E_h^J / \tilde{E}_l^J)^M$, where M denotes the number of links on the inner boundary (this estimate applies to the 'optimal' dimer configuration shown in Fig. 4). Hence introducing one switchable link junction near the inner boundary allows us to tune the parameter \tilde{E}_l^J and change the mixing amplitude h_x by many orders of magnitude. The variant for the JJK array involves a virtual excitation with two Cooper pairs on one hexagon.

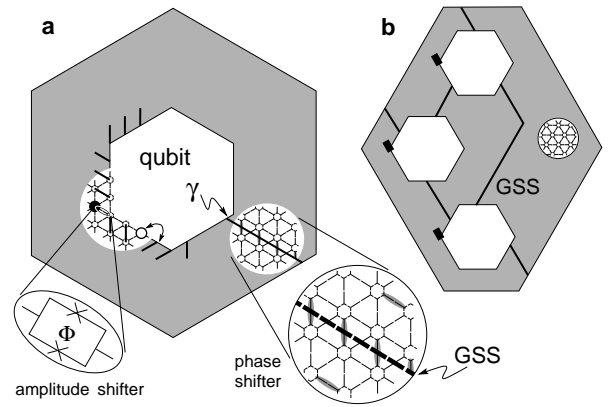


FIG. 4. **a** The topologically protected qubit involves the two degenerate groundstates of the quantum dimer liquid state realized within a triangular Josephson junction array. The qubit's phase is manipulated through the gated superconducting strip (GSS) attracting dimers along γ . The amplitude shifter mixing the groundstates is realized with the help of a tunable Josephson junction placed at the inner qubit boundary. Dimer-flips, like a row of falling dominos, take the hole around the inner boundary. **b** Array of topologically protected qubits embedded in a Josephson junction array emulating a dimer system. The entanglement of two qubits proceeds through coupling over a gated superconducting strip.

The 'phase shifter' can be implemented through a gated superconducting strip, capacitively coupled to the array and attracting dimers onto the reference line γ . Upon biasing the strip, the energies of the two groundstates are shifted with respect to one another and the qubit's phase χ is modified accordingly. The implementation requires careful adiabatic switching, with the amplitude u (the energy acting on one dimer) and the duration τ of the manipulation limited by the constraints $u \sim t \ll E_l^J$ and $\tau > \hbar/\Delta$ in order to avoid excitations within the dimer liquid. Furthermore, we have to break up the strip during idle time, as the fully connected strip represents a global operator (otherwise, electric fluctuations fed to the strip would decohere the system). Thus the strip has to be constructed from isolated superconducting islands which are to be connected only during the time where the phase shifter becomes operational. Fast switches accomplishing such a connection can be built from superconducting Cooper pair transistors [25].

The qubit's manipulation involve strong modifications of the system: the amplitude shifter requires leaving the protected Hilbert space through virtual breaking of a dimer, while the phase shifter requires introduction of a global operator. In turn, these processes are strongly inhibited during idle time and give the qubit its robustness: amplitude mixing is exponentially small in L_x while phase drifting is exponentially small in L_y , cf. (4).

Constructing a register of qubits is surprisingly simple: the same basic Josephson junction array can accommodate K qubits in a geometry with K holes, see Fig. 4. Individual qubit operations are carried out as described

above. The implementation of a non-trivial two-qubit operation again involves a superconducting strip: biasing the strip connecting two qubits lifts the energy of the states $|eo\rangle$ and $|oe\rangle$ with respect to the states $|ee\rangle$ and $|oo\rangle$ and combining this two-qubit ‘phase shifter’ with a suitable set of single qubit operations allows for the construction of the controlled-NOT operation [8].

In a first step towards the implementation of topologically protected qubits one may wish to test the proper functionality of the quantum Josephson junction array. Such a test is provided by a measurement of the magnetic susceptibility χ of the ring-shaped structure: applying a magnetic field, the mixing energy h_x picks up a factor $\cos(2\pi\Phi/\Phi_0)$, where $\Phi_0 = hc/e$ is the normal state flux quantum. This factor originates from the Aharonov-Bohm phase picked up by the virtual charged excitations encircling the hole. In the absence of disorder the ring’s energy changes with flux, $E_{\text{ring}}(\Phi) = h_x |\cos(2\pi\Phi/\Phi_0)|$, resulting in a susceptibility $\chi \propto \partial_\Phi^2 E_{\text{ring}}$ with period $\Phi_0/2$ and a sharp feature at $\Phi = \Phi_0/4$. The splitting Δ_d in the groundstate energies (due to disorder or finite-size effects) smears this sharp feature over a region $\delta\Phi/\Phi_0 \sim \Delta_d/h_x$; hence a measurement of $\chi(\Phi)$ allows to check on the mixing amplitude h_x and on the level splitting.

A particular challenge faced by qubit implementations based on Josephson junctions operating in the charge limit is the presence of stray charges [5,9]; the robustness in our device efficiently suppresses fluctuations in the gate potential once they drop below t . The problem of stray charges is avoided in designs using the dual phase variable [7,8,11] and work in this direction is in progress.

We thank V. Geshkenbein for discussions and acknowledge financial support through the SCOPES program (swiss federal department of foreign affairs and SNF), the NWO-Russia collaboration program, the RFBR grant 01-02-17759, the program ‘Quantum Macrophysics’ of the Russian Academy of Science, and the Russian Ministry of Science. Computations have been carried out on the Beowulfcluster Asgard at ETHZ.

[1] Cirac, J.I. & Zoller, P. Quantum computations with cold trapped ions. *Phys. Rev. Lett.* **74**, 4091-4094 (1995).
[2] Monroe, C., Meekhof, D., King, B., Itano, W. & Wineland, D. Demonstration of a fundamental quantum logic gate. *Phys. Rev. Lett.* **75**, 4714-4717 (1995).
[3] Turchette, Q., Hood, C., Lange, W., Mabushi, H. & Kimble, H.J. Measurement of conditional phase shifts for quantum logics. *Phys. Rev. Lett.* **75**, 4710-4713 (1995).
[4] Loss, D. & DiVincenzo, D.P. Quantum computation with quantum dots. *Phys. Rev. A* **57**, 120-126 (1998).
[5] Shnirman, A., Schön, G. & Hermon, Z. Quantum manipulations of small Josephson junctions. *Phys. Rev. Lett.* **79**, 2371-2374 (1997).

[6] Averin, D.V. Adiabatic quantum computation with Cooper pairs. *Solid State Commun.* **105**, 659-664 (1998).
[7] Mooij, J.E., Orlando, T.P., Levitov, L.S., Tian, L., van der Wal, C.H. & Lloyd, S. Josephson persistent-current qubit. *Science* **235**, 1036-1039 (1999).
[8] Ioffe, L., Geshkenbein, V.B., Feigel’man, M.V., Fauchère, A.L. & Blatter, G. Environmentally decoupled s -wave- d -wave- s -wave Josephson junctions for quantum computing. *Nature* **398**, 678-681 (1999).
[9] Nakamura, Y., Pashkin, Yu.A. & Tsai, J.S. Coherent control of macroscopic quantum states in a single-Cooper-pair box. *Nature* **398**, 786-788 (1999).
[10] Friedman, J.R., Patel, V., Chen, W., Tolpygo, S.K. & Lukens, J.E. Quantum superposition of distinct macroscopic states. *Nature* **406**, 43-46 (2000).
[11] van der Wal, C.H., ter Haar, A.C.J., Wilhelm, F.K., Schouten, R.N., Harmans, C.J.P.M., Orlando, T.P., Lloyd, S. & Mooij, J.E. Quantum superposition of macroscopic persistent-current states. *Science* **290**, 773-777 (2000).
[12] Kitaev, A.Yu. Fault-tolerant quantum computation by anyons. quant-ph/9707021.
[13] Preskill, J. Fault-tolerant quantum computation. *Introduction to quantum computation and information* (World Scientific, Singapore, 1998).
[14] Kivelson, S.A., Rokhsar, D.S. & Sethna, J.P. Topology of the resonating valence-bond state: solitons and high- T_c superconductivity. *Phys. Rev. B* **35**, 8865-8868 (1987).
[15] Rokhsar, D.S. & Kivelson, S.A. Superconductivity and the quantum hard-core dimer gas. *Phys. Rev. Lett.* **61**, 2376-2379 (1988).
[16] Wen, X.G. Mean-field theory of spin-liquid states with finite energy gap and topological orders. *Phys. Rev. B* **44**, 2664-2672 (1991).
[17] R. Moessner, R. & Sondhi, S.L. Resonating valence bond phase in the triangular lattice quantum dimer model. *Phys. Rev. Lett.* **86**, 1881-1884 (2001).
[18] Misguich, G., Lhuillier, C., Bernu, B. & Waldtmann, C. Spin-liquid phase of the multiple-spin exchange Hamiltonian on the triangular lattice. *Phys. Rev. B* **60**, 1064-1074 (1999).
[19] Sachdev, S. Kagome-acute- and triangular-lattice Heisenberg antiferromagnets. *Phys. Rev. B* **45**, 12377 (1992).
[20] Fradkin, E. *Field Theories of Condensed Matter Systems*. Addison-Wesley, Redwood City, CA, 1991.
[21] Moessner, R., Sondhi, S.L. & Fradkin, E. Short-ranged RVB physics, quantum dimer models and Ising gauge theories. cond-mat/0103396.
[22] Anderson, P.W. The resonating valence bond state in La_2CuO_4 and superconductivity. *Science* **235**, 1196-1198 (1987).
[23] Ioffe, L.B. & Larkin, A.I. Superconductivity in the liquid-dimer valence-bond state. *Phys. Rev. B* **40**, 6941-6947 (1989).
[24] Fradkin, E. & Shenker, S.H. Phase diagrams of lattice gauge theories with Higgs fields. *Phys. Rev. D* **19**, 3682 (1979).
[25] Grabert, H. & Devoret, M.H. *Single charge tunneling: coulomb blockade phenomena in nanostructures*. Plenum Press, New York, 1992.